Plasma Sources Sci. Technol. **17** (2008) 035017 (13pp) doi:10.1088/0963-0252/17/3/035017

Two-dimensional fluid model of a two-chamber plasma source

St Kolev[1], A Shivarova[1], Kh Tarnev[2] and Ts Tsankov[1]

[1] Faculty of Physics, Sofia University, BG-1164 Sofia, Bulgaria
[2] Department of Applied Physics, Technical University-Sofia, BG-1000 Sofia, Bulgaria

E-mail: ashiva@phys.uni-sofia.bg

Received 9 November 2007, in final form 22 April 2008
Published 7 July 2008
Online at stacks.iop.org/PSST/17/035017

Abstract
This study presents a two-dimensional fluid-plasma model developed for describing the cw regime operation of a tandem plasma source, consisting of a driver and an expansion plasma volume of different sizes. The moderate pressure range considered (tens to hundreds of milliTorr) allows a description within the drift–diffusion approximation, as employed in the model. Argon discharges maintained in a metal gas-discharge vessel are treated. The discussions stress charged-particle and electron-energy fluxes as well as the spatial distribution of their components. The main conclusions are for (i) different electron and ion fluxes resulting in a net current in the discharge; (ii) a radial ion flux prevailing over the axial one and an axial electron flux prevailing over the radial one; (iii) ion motion determined by the dc electric field and drift–diffusion electron motion influenced by thermal diffusion; (iv) plasma maintenance in the expansion plasma chamber due to charged-particle and electron-energy fluxes from the driver; (v) importance of the convective flux in the electron-energy balance; (vi) electron-energy losses for sustaining the dc electric field in the expansion plasma volume strongly predominating over the losses through collisions and (vii) electron cooling accompanied by a strong drop in the plasma density and in the potential of the dc electric field, due to the plasma expansion in a bigger volume. In general, the results show that the gas pressure range usually considered to be governed by ambipolar diffusion shows up in a different regime: a regime with a dc current, when the discharge is in a metal chamber with different dimensions in the transverse and longitudinal directions.

1. Introduction

One-dimensional models of gas discharges sustained in long gas discharge tubes or between flat electrodes have traced out the basis of gas discharge physics. However, they could not meet the recent and current requirements for design and optimization of plasma sources [1–10] developed for microelectronics-processing and surface-modification technologies as well as for use as particle sources. The complicated geometry of these sources as well as their design with electrodes and walls of different materials and their operation in different modes (cw and pulsed regimes) require a description based on at least two-dimensional (2D) models, nowadays possible due to increased computational capabilities. In general, the discharge vessels of the rf reactors for plasma processing and of the rf plasma-based particle sources are completed by two chambers and, respectively, the discharge consists of two regions with different types of plasma behaviour. The first region is the driver, where the external power is deposited. Discharge maintenance in the second region is due to plasma expansion from the driver. For this reason the two-chamber plasma sources are called remote plasma sources [2] in the literature on the technological applications of the discharges, or tandem plasma sources [11] in the literature on negative hydrogen ion beams. The latter stresses space separation of plasmas of different electron temperatures (higher electron temperature in the driver and a low one in the expansion plasma volume) usually achieved by magnetic filters. Different types of discharges—inductive and capacitive discharges, studied separately or as different modes of the operation of the Gaseous Electronics Conference rf Reference Cell [3, 4, 6, 8, 12–14], as well as helicon discharges [15, 16]—have been studied. The studies also cover discharge maintenance in different gases: more

often noble gases [3–6, 9, 13–19] but also oxygen [5, 18] and gas mixtures [2, 5, 14, 17–19]—Ar/Cl_2, $Ar/H_2 + SiH_4$, $He-SiH_4$, $Ar/CF_4/O_2$, etc—of interest for the plasma processing technologies. The results accumulated are for the spatial distribution of the basic plasma parameters (electron density and temperature) as well as of the concentration of the different species in discharges in gas mixtures. Strong variations of this distribution both in the driver and in the expanding plasma volume have been shown with changes in the size of the two chambers and of the wall material (metal/dielectric walls) or due to magnetic fields and grounded electrodes modifying the discharge performance. Regardless of the information accumulated, the plasma behaviour in sources with an expansion plasma volume is a field open for research, due to the complexity of the problem.

This study presents a fluid-plasma 2D model describing the spatial structure of the discharge characteristics in a tandem plasma source with metal walls sustaining an argon discharge in the gas pressure range of the diffusion-controlled regime. The detailed analysis of the charged-particle and electron-energy fluxes shows that the discharge behaviour completely deviates from the ambipolar-diffusion regime, i.e. ions and electrons flow in different directions. Axial electron flux and radial ion flux short-circuited through the metal walls and resulting in a net current in the plasma remind us of Simon diffusion [10, 20], well known in the literature as being diffusion in discharges in metal chambers, however, when the discharge is in an external magnetic field. In high-frequency sources of unmagnetized plasma production the regime with a dc current flowing through the discharge results from metal walls of the source combined with different dimensions of the discharge vessel in its longitudinal and transverse directions. The ion motion is a drift motion in the dc electric field. Drift–diffusion motion influenced by thermal diffusion forms the electron flux. Sustained by charged-particle and electron-energy fluxes from the driver, the plasma in the expanding plasma region has a quite lower electron temperature and density than those in the driver. Whereas the inelastic collisions for excitation are the main contributor to the electron-energy losses in the driver, the electron-energy losses for the maintenance of the dc electric field in the expansion plasma volume strongly exceed the losses through collisions.

The geometry of the source, the initial set of equations involved in its description as well as the gas discharge conditions considered are given in section 2. Sections 3 and 4 present the results from the model: for the spatial distribution of the plasma parameters (section 3) and of the charged-particle and electron-energy fluxes (section 4). The results shown in section 5 contribute to outlining the main conclusions from the model: the geometry of the source in combination with its metal walls establishes in the gas pressure range of the diffusion-controlled high-frequency discharges a gas discharge regime with a net dc current flowing across the discharge vessel.

2. Formulation of the problem, initial set of equations and gas discharge conditions

By developing the 2D fluid-plasma model presented here, we have had in mind the description of the spatial structure of discharges sustained in the tandem plasma sources studied with regard to their use as rf-driven sources of negative hydrogen ions [21] for additional heating of tokamak plasmas. However, aiming at the description of the main trends of the operation of the sources, shown experimentally [22] to be similar in hydrogen and argon, the discharge considered here is in an argon gas, a simpler gas compared with hydrogen.

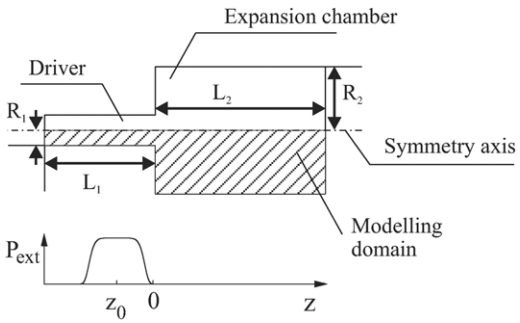

Figure 1. Schematic representation of the configuration of the source and of the modelling domain. The zero position on the z-axis is at the transition between the driver and the expanding plasma volume. The location of the input power is also given.

The source (figure 1) is a two-chamber source with metal walls consisting of a driver region of a smaller size and an expanding plasma volume of a bigger size. The z-axis is along the length of the source. The zero z-position is at the transition between the two chambers of the source, i.e. between the driver and the expanding plasma volume. Thus, negative z-values correspond to positions in the smaller size chamber where the driver is located.

The rf power input P_{ext} to the driver region is assumed radially constant, with a super-Gaussian profile in the z-direction:

$$P_{\mathrm{ext}} = P_0 \exp\left[-\frac{1}{2}\left(\frac{z - z_0}{\sigma}\right)^{2m}\right] \tag{1}$$

centred at $z = z_0$, with a value of P_0 there ($P_0 = P_{\mathrm{ext}}(z = z_0)$) and σ scaling its width. The values of z_0 and σ chosen do not permit penetration of external power into the expansion plasma volume.

The CW regime of discharge maintenance in the gas pressure range between tens and hundreds of milliTorr is studied by applying the drift–diffusion approximation. The initial set of equations solved numerically by using the finite element method consists of the continuity equations for the electrons and ions

$$\mathrm{div}\boldsymbol{\Gamma}_{\mathrm{e,i}} = \frac{\delta n_{\mathrm{e,i}}}{\delta t}, \tag{2}$$

the electron-energy balance equation

$$\mathrm{div}\,\boldsymbol{J} = P_{\mathrm{ext}} - e\boldsymbol{\Gamma}_{\mathrm{e}} \cdot \boldsymbol{E} + P_{\mathrm{coll}} \tag{3}$$

and the Poisson equation

$$\triangle\Phi = \frac{e}{\epsilon_0}(n_{\mathrm{e}} - n_{\mathrm{i}}). \tag{4}$$

Here $n_{e,i}$ and $\mathbf{\Gamma}_{e,i}$ are, respectively, the densities and the fluxes of the electrons and ions, $\delta n_{e,i}/\delta t$ describe the charged particle production in ionization, $\boldsymbol{J}$ is the electron-energy flux, P_{coll} includes the electron-energy losses in collisions, $\boldsymbol{E}$ is the dc electric field in the discharge and Φ is its potential ($\boldsymbol{E} = -\nabla\Phi$), e is the electron charge and ϵ_0 is the vacuum permittivity. The charged particle fluxes obtained from the momentum equations of the electrons and ions are, respectively:

$$\mathbf{\Gamma}_e = -b_e n_e \boldsymbol{E} - D_e \nabla n_e - D_e^T n_e \frac{\nabla T_e}{T_e}, \tag{5a}$$

$$\mathbf{\Gamma}_i = b_i n_i \boldsymbol{E} - D_i \nabla n_i, \tag{5b}$$

where

$$b_e = \frac{e}{\mu_{en}\nu_{en}}, \qquad b_i = \frac{e}{\mu_{in}\nu_{in} + \dfrac{m_i}{n_i}\dfrac{\delta n_i}{\delta t}}$$

and

$$D_e = \frac{T_e}{\mu_{en}\nu_{en}}, \qquad D_i = \frac{T_i}{\mu_{in}\nu_{in} + \dfrac{m_i}{n_i}\dfrac{\delta n_i}{\delta t}}$$

are, respectively, the mobilities $b_{e,i}$ and the diffusion coefficients $D_{e,i}$ of electrons and ions; $D_e^T \equiv D_e$ is the thermal diffusion coefficient of the electrons and $T_{e,i}$ are the electron and ion temperatures ($T_i \equiv T_g = \text{const.}$ with T_g being the gas temperature). Whereas only elastic electron–neutral collisions (with frequency ν_{en} and reduced mass μ_{en}) are taken into account in the momentum equation of the electrons, the ion momentum equation involves both elastic collisions (ν_{in} and μ_{in} are their frequency and reduced mass) and inelastic collisions, as given by the second terms in the denominators of b_i and D_i; m_i is the ion mass. Accounting for an effective mobility and, respectively, an effective diffusion coefficient of the ions extends the validity of the model to lower gas pressures.

The electron-energy flux $\boldsymbol{J}$

$$\boldsymbol{J} = -\chi_e \nabla T_e + \frac{5}{2} T_e \mathbf{\Gamma}_e \tag{6}$$

involved in (3) includes both the conductive (thermal) flux $\boldsymbol{J}^{(cond)} = -\chi_e \nabla T_e$ ($\chi_e = \frac{5}{2} n_e D_e$ is the thermal conductivity coefficient) and the convective flux $\boldsymbol{J}^{(conv)} = \frac{5}{2} T_e \mathbf{\Gamma}_e$. The latter accounts for thermal energy and pressure force work carried by the directed velocity of the electrons. With the second term on the left-hand side of (3), the electron losses for maintenance of the dc electric field in the discharge are taken into account. The electron-energy losses P_{coll} in collisions

$$P_{coll} = -n_e \nu_* U_* - n_e \nu_i U_i - \frac{3}{2}\delta \nu_{en} n_e T_e \tag{7}$$

involve losses in inelastic collisions for (total) excitation and direct ionization, as given by the first two terms in (7), as well as losses in elastic electron–neutral collisions (the third term in (7)); ν_*, ν_i and ν_{en} are the corresponding collision frequencies, U_* and U_i are, respectively, the energy of the first atom excited state and the ionization energy and $\delta = 2m_e/m_a$ (with m_e and m_a being, respectively, the electron and atom masses) is the portion of energy transferred by the electron to the atom in an elastic collision.

The charged particle production in (2)

$$\frac{\delta n_{e,i}}{\delta t} = \left(\frac{\delta n_{e,i}}{\delta t}\right)_d + \left(\frac{\delta n_{e,i}}{\delta t}\right)_{st} \tag{8}$$

is via direct ionization $(\delta n_{e,i}/\delta t)_d = \nu_i n_e$ and step ionization $(\delta n_{e,i}/\delta t)_{st} = k_{ji} N_j n_e$ from the first four atom excited states ($^3P_0$, $^3P_2$, $^1P_1$ and $^3P_1$) considered as a block; k_{ji} is the corresponding rate coefficient and N_j is the concentration of the excited atoms. Accounting for the step ionization involves in the model the balance equation of the excited atoms

$$\text{div}\mathbf{\Gamma}_j = \frac{\delta N_j}{\delta t}, \tag{9}$$

where

$$\mathbf{\Gamma}_j = -D_j \nabla N_j \tag{10a}$$

is their flux (D_j is the diffusion coefficient) and

$$\frac{\delta N_j}{\delta t} = k_{0j} N_0 n_e - (k_{ji} + k_{j0}) N_j n_e \tag{10b}$$

describes their production by population from the ground state (the first term on the right-hand side of (10*b*) with N_0 being the ground state atom density) and losses via ionization and transitions to the ground state (with a rate coefficient k_{j0}).

The boundary conditions for the fluxes at the walls are those [3, 4, 23] usually used:

$$\boldsymbol{n} \cdot \mathbf{\Gamma}_e = \frac{1}{4} v_{th,e} n_e \tag{11a}$$

for the electron flux ($v_{th,e}$ is the electron thermal velocity),

$$\boldsymbol{n} \cdot \mathbf{\Gamma}_i = \frac{1}{2} v_{th,i} n_i + b_i n_i (\boldsymbol{n} \cdot \boldsymbol{E}) \tag{11b}$$

for the ion flux ($v_{th,i}$ is the ion thermal velocity),

$$\boldsymbol{n} \cdot \mathbf{\Gamma}_j = \frac{1-\gamma}{2(1+\gamma)} v_{th,j} N_j \tag{11c}$$

for the flux of the excited atoms ($v_{th,j}$ is their thermal velocity and γ is the coefficient of their reflection from the walls) and

$$\boldsymbol{n} \cdot \boldsymbol{J} = \frac{5}{2} T_e (\boldsymbol{n} \cdot \mathbf{\Gamma}_e) \tag{11d}$$

for the electron-energy flux. In (11*a*)–(11*d*), $\boldsymbol{n}$ is the unit vector, normal and directed towards the walls. The boundary condition for the potential of the dc electric field is for grounded metal walls ($\Phi = 0$ at the walls).

The symmetry at the axis of the source ($r = 0$) implies that the radial components of the particle and electron-energy fluxes and of the dc electric field are equal to zero ($\Gamma_{\alpha r}(r = 0) = 0$, $J_r(r = 0) = 0$ and $\frac{d\Phi}{dr}(r = 0) = 0$; $\alpha = e, i, j$). With boundary conditions taken at $r = 0$, the calculations cover half of the source denoted as a modelling domain in figure 1.

The continuity equations (2) of both electrons and ions are present in the set of equations solved. This means that in the model, in general, the electron and ion fluxes could be different

($\mathbf{\Gamma}_e \neq \mathbf{\Gamma}_i$). However, the condition div$\mathbf{\Gamma} = 0$, with $\mathbf{\Gamma} = \mathbf{\Gamma}_e - \mathbf{\Gamma}_i$, always holds since each act of ionization simultaneously produces an electron and an ion ($\delta n_e/\delta t = \delta n_i/\delta t$ in (2)). Obtaining $\mathbf{\Gamma}_e \neq \mathbf{\Gamma}_i$ means the existence of a discharge regime different from the ambipolar-diffusion regime in the pressure range of the diffusion-controlled discharges.

The obtained numerical solutions of the set of equations (2)–(4) and (9), with the above given boundary conditions, are for the spatial structure of the discharge in the source given in figure 1. The size of the source is the same as that of the discharge vessel at the experimental set-up [22, 24–27] constructed with regard to small-scale experiments on hydrogen discharges as sources of negative hydrogen ions: radius $R_1 = 2.25$ cm and length $L_1 = 30$ cm of the first chamber, where the driver region is located, and, respectively, $R_2 = 11$ cm and $L_2 = 47$ cm of the second chamber, which provides the large volume for plasma expansion from the driver.

The discharge is in an argon gas. The collision frequencies and the rate coefficients of the processes included in the charged-particle and electron-energy balance are calculated as described in [28, 29]; the coefficient γ in (11c) is taken with a value of $\gamma = 0.1$.

The complete set of results presented is for a gas pressure $p = 100$ mTorr. Results for $p = 50$ mTorr are also shown with regard to discussions on the influence of gas pressure variation.

In all the cases the value of the total power applied for the discharge maintenance is 100 W. The parameters of the super-Gaussian profile (1) of the applied power are $z_0 = -10$ cm, $\sigma = 7.2$ cm and $m = 4$. In order to avoid penetration of the applied power in the expanding plasma volume ($z > 0$) by the wing of the super-Gaussian profile at z approaching zero, $P_{ext}(z \geqslant 0) = 0$ is additionally imposed.

The power input is locally applied in the first chamber. This means that the plasma existence in the total volume of the discharge vessel could be provided by plasma expansion beyond the region of the localization of the input power. Thus, the discharge regime is under the conditions of strong nonlocality, both with respect to the charged particle balance and the electron-energy balance. Under such conditions, the specific shape of the spatial distribution of the input power cannot influence the discharge regime. An analogy could be drawn with the radial distribution of the plasma parameters of discharges maintained in long gas discharge tubes: when nonlocality in heating holds [30, 31], the electron temperature stays almost constant across the radius, independently of the radial distribution of the input power. In general, in the source considered here—with power deposition in the first chamber and plasma expansion in the second one—the charged-particle and the electron-energy fluxes should play an important role, as shown by the results presented in the following sections.

With a length of approximately 15 cm of the power input region centred at $z_0 = -10$ cm, the plasma expands in both the second—bigger—chamber and in the first—smaller—chamber, in the region $-30\,\text{cm} \lesssim z \lesssim -20\,\text{cm}$ towards its back wall ($z = -30$ cm). The results for the spatial distribution of the plasma parameters on both sides of the driver provide possibilities for comparison of the behaviour

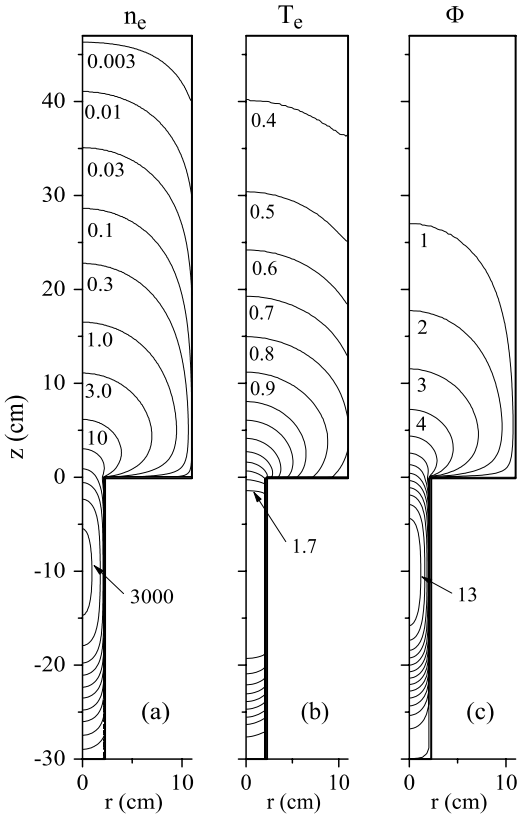

Figure 2. Contours of constant (a) electron density in [10^{15} m^{-3}], (b) electron temperature in [eV] and (c) potential of the dc field in [V]; $p = 100$ mTorr.

of plasmas expanding in volumes of different sizes (radius of the expansion region larger or equal to that of the driver). The discussions stress that diffusion-controlled discharges are maintained under the conditions of different electron and ion fluxes even without an external magnetic field, when the discharge is in a metal chamber with different characteristic lengths in the axial and transverse directions.

3. Spatial distribution of the plasma parameters

The contour plots in figure 2 as well as the axial and radial profiles presented, respectively, in figures 3 and 4 show the spatial distribution of the electron density and temperature and of the potential of the dc field.

The region of the power input—the driver region—appears very well outlined by the highest ($T_e = 1.7$ eV) contour in figure 2(b). The electron density and the potential of the dc field (figures 2(a) and (c)), having their highest values in the driver also, decrease strongly both in the axial and radial directions, with the radial gradients bigger than the axial ones. With regard to the dc electric field this means a larger radial component (except for the region around the discharge axis ($r = 0$)) and predominating field orientation perpendicularly to the walls.

The variation of the plasma parameters towards the positive z-values shows that electron cooling and a strong decrease in the electron density and in the dc potential characterize the plasma expansion in a bigger volume. The

highest axial gradients of n_e and Φ and, respectively, the fastest axial variations are at the transition between the two chambers of the discharge vessel. The same also holds for the electron temperature.

The changes in the plasma parameters in the region $-30\,\text{cm} \lesssim z \lesssim -20\,\text{cm}$ on the other side of the driver, with respect to the second chamber, show the behaviour of plasmas expanding in a small-size discharge vessel, in our case a discharge vessel of the same size as that of the driver. The contour plots in figure 2 as well as the axial profiles in figure 3 show a stronger decrease in n_e, T_e and Φ when the plasma expands in a small diameter tube. Whereas for $z > -10\,\text{cm}$, i.e. towards the large volume expansion region, the fast drop in the plasma parameters formed at the edge of the power input region transfers into smoother variations at the beginning of the second chamber, on the other side of the driver, towards $z \to -30\,\text{cm}$, the strong gradients of the plasma parameters stay the same over the whole distance to the back wall of the small diameter vessel. As pointed out in [22], the experiments also show a stronger drop in the plasma parameters—compared with that in a larger volume expanding plasma vessel—when the size of the expanding plasma vessel is the same as that of the driver.

These results on the behaviour of the plasma expansion in large and small diameter volumes lead to the point that the smaller radial diffusion losses of charged particles in a larger-diameter discharge vessel determine smoother axial profiles of the plasma parameters.

A closer look at the axial profile of the electron temperature (figure 3(*b*)) shows its slight variation in the driver region with the formation of maxima close to the edges of the power input region, on both sides of its centre ($z = -10\,\text{cm}$). Deep inside the second chamber, the axial decrease in T_e (figure 3(*b*)) is slow, compared with the exponential drop in the plasma density (figure 3(*a*)).

Figure 3 shows that decreasing gas pressure leads to an increase in the electron temperature and to a decrease in the electron density. The dc potential in the driver region also increases. Such changes in the plasma parameters with the gas-pressure variation are in accordance with the expectations from the well-established knowledge [20] on the maintenance of gas discharges by power deposition to the total volume of the discharge. Increased diffusion losses due to the gas pressure decrease leads to an increase in the electron temperature (and, respectively, in the dc potential) and to a decrease in the plasma density when the input power is kept constant. In the expanding plasma regions (both of bigger size and of the same size as of the driver), the changes in the electron temperature and density with varying gas pressure are the same as in the driver: the electron temperature is higher and the electron density is lower for lower gas pressure (figures 3(*a*) and (*b*)). However, deep in the expanding plasma regions on both sides of the driver, the plasma potential is higher for higher gas pressure.

Figure 4 shows normalized radial profiles of the plasma density in the driver (at its centre $z = -10\,\text{cm}$) and in the expanding plasma regions on both sides of the driver (respectively, $z = -25\,\text{cm}$ and $z = 1$, 5 and 30 cm); the normalization is to the corresponding values at the discharge axis ($r = 0$).

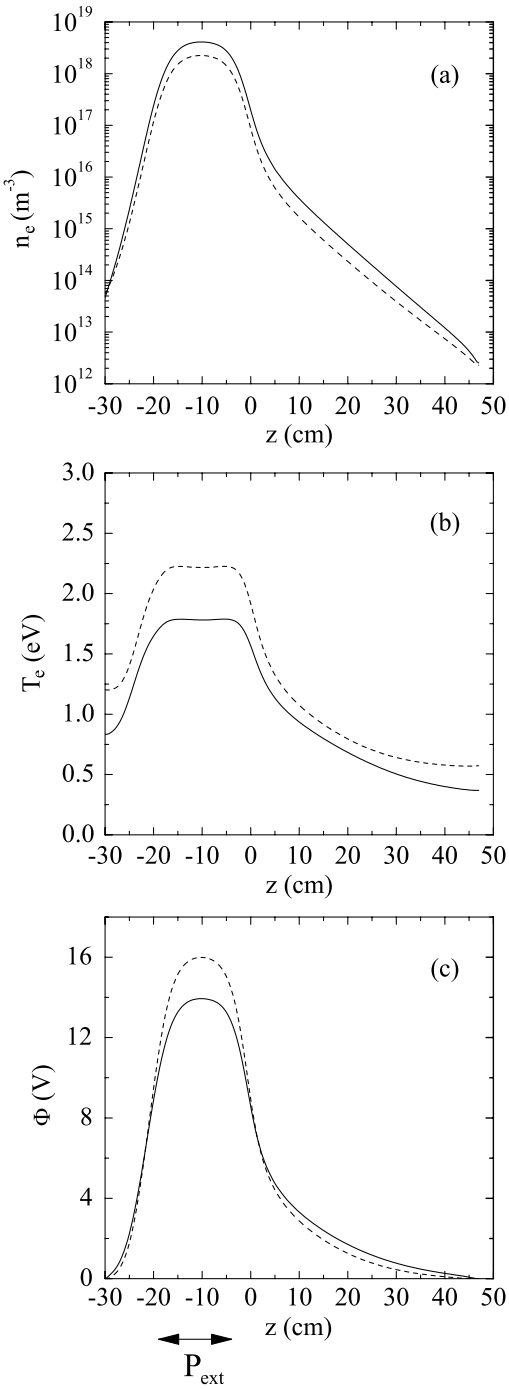

Figure 3. Axial profiles, at the centre ($r = 0$) of the vessel, of the electron density and temperature, respectively, in (*a*) and (*b*) and of the potential of the dc electric field in (c), for two values of the gas pressure: solid curves for $p = 100\,\text{mTorr}$ and dashed curves for $p = 50\,\text{mTorr}$. The arrows below (*c*) mark the position of the power input region.

In the centre ($z = -10\,\text{cm}$) of the driver as well as deep in the expansion plasma region ($z = 30\,\text{cm}$) in the second chamber, away from both the transition between the two chambers and the back wall of the second chamber ($z = 47\,\text{cm}$), the radial profiles of the electron density could be very well approximated by a Bessel function profile

$$n_e(r) = n_e(r = 0) J_0\left(\frac{\mu}{R} r\right), \tag{12}$$

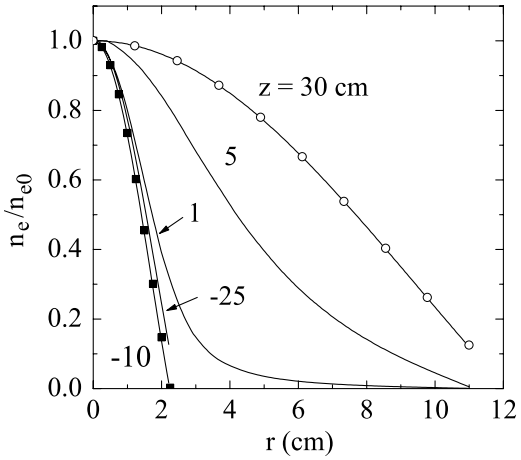

Figure 4. Radial profiles, at different axial positions as denoted in the figure, of the electron density, normalized to its values at the axis ($r = 0$) of the discharge vessel, for the given z-value; $p = 100$ mTorr. The negative z-positions are in the first chamber (of radius $R_1 = 2.25$ cm) and the positive ones are in the second chamber (of radius $R_2 = 11$ cm). The symbols show approximation of the profiles at $z = -10$ cm and $z = 30$ cm with the Bessel function $J_0(\mu r/R)$ with values of the parameter μ, respectively, $\mu = 2.37$ and $\mu = 2.175$ for $R \equiv R_1 = 2.25$ cm and $R \equiv R_2 = 11$ cm.

where J_0 is the zeroth-order Bessel function. The values of the parameter μ of the Bessel profiles are $\mu = 2.37$ for $z = -10$ cm and $\mu = 2.175$ for $z = 30$ cm. The latter is also the value of μ of the profile for $z = -25$ cm. A value of μ different from $\mu = 2.405$ means a nonzero value of the plasma density at the walls, which is the actual situation since it ensures a nonzero flux at the walls for a finite velocity of the charged particles. Although the normalized densities at the discharge walls for $z = -25$ cm and 30 cm are the highest ones in figure 4, due to the low densities at the discharge axis away from the driver, the absolute values of the densities at these axial positions are the lowest ones.

Good approximation—by a Bessel function—of the radial profiles of the plasma density in the centre of the driver and away from it, deep in the expanding plasma volume, means that analytical solutions in these regions of the charged particles' balance equation (2) of the type of solutions with separated variables $n(r, z) = n_r(r)n_z(z)$ are possible. This is confirmed not only by the Bessel function approximations of the radial profiles of the plasma density shown in figure 4 but also by the cosine-type of its axial profile in the driver region (-20 cm $\leqslant z \lesssim 0$ cm) and its exponential drop deep inside the expansion plasma region (figure 3(*a*)). The axial density profiles in these two regions would be, respectively, a cosine- and exponential-type of functions provided that there is a strong ionization in the driver and there is no ionization in the expanding plasma region. Moreover, in the case of a step ionization, the latter should be with a strong saturation in order to have the continuity equation (2) in the form of a linear differential equation. In addition, separation of the variables in the continuity equation (2) would be possible if the thermal diffusion in (5*a*) and, respectively, the spatial variations of T_e could be neglected. The obtained numerical solutions show that all these approximations are at least roughly fulfilled. The results in the next subsection show that (i) in the driver region the ionization is strong (predominating strongly saturated step ionization) whereas in the expansion plasma volume of the second chamber it is negligibly small, (ii) the spatial variations of T_e in the driver region are very weak (figure 3(*b*)), and T_e could be considered as a constant there, and (iii) although having well-pronounced variations of T_e deep in the expanding plasma region (figure 3(*b*)), a rough approximation to a constant T_e is acceptable. The good approximation of the radial variations of the electron density to the Bessel type of profile shown does not contradict the result for different fluxes of electrons and ions stressed in the next section.

The central part of the radial profile of the plasma density at $z = 1$ cm (figure 4), a position in the second chamber close to its front wall ($z = 0$ cm), still reminds us of its distribution in the first chamber. The completely different shape of the profile over the distance between the radii of the first and second chamber is obviously due to the strong impact of the front wall of the second chamber, respectively, the strong effect of charged-particle and electron-energy backward axial fluxes towards this wall. The radial profile depicted at $z = 5$ cm shows a smooth transition towards the region in the second chamber away from its front wall, where the plasma-parameter behaviour is determined by radial and forward axial fluxes.

In the driver region where T_e is almost constant the Boltzmann relation between n_e and Φ is well satisfied. In the expansion plasma region the Boltzmann relation could also be considered as an approximation; however, only over short z-intervals, because of the axial variation of T_e.

In connection with the fluxes presented in the next section attention should also be paid to the weak maxima in the axial (figure 3(*b*)) profile of T_e in the driver region which appear close to the edges of the power input region. The radial T_e-profile also shows up with a maximum close to the wall. Although very weak, these maxima appear to be important since their presence causes backward—in the radial direction towards the axis and in the axial direction towards the central part of the driver—thermal and thermal-diffusion fluxes. The reason for their appearance is a combined effect of the decrease in the plasma density, both in the radial direction towards the wall (figure 4) and in the axial direction at the edges of the driver region (figure 3(*a*)), with the constant input power (in the radial direction and in the axial one over the plateau of its super-Gaussian axial profile). The radially constant power input is an assumption in the model, but it should be stressed that the situation would be the same for, e.g., an inductively driven discharge. With the high maximum of the power deposition close to the walls in inductive discharges [28], the maximum in the radial T_e profile would be even better pronounced. Due to the edge effects in the axial direction—on both sides of the coil driving the inductive discharge—which will always be present in a 2D modelling of the power deposition, the maxima in the axial profile of T_e will also be kept.

4. Charged-particle and electron-energy fluxes

With the localized power input, the plasma existence in the regions of the source outside the driver is due to charged-particle and electron-energy fluxes from the driver. Therefore, the pattern of these fluxes stressed in this section gives indications about the manner of the operation of the source. The complicated design of the source, with a small-radius driver and a large-radius expanding plasma volume, gives rise to many questions requiring a detailed description of the fluxes. Such a basic question is, for example, whether the plasma in the expanding plasma volume exists due to charged-particle fluxes from the driver or it is produced there owing to electron-energy flux from the driver. In addition, the different electron and ion fluxes obtained ($\mathbf{\Gamma}_e \neq \mathbf{\Gamma}_i$) due to the metal walls of the chamber and its different dimensions in the longitudinal and transverse directions need unravelling the pattern of the fluxes in order to clarify the role in the source operation of the flux $\mathbf{\Gamma} = \mathbf{\Gamma}_e - \mathbf{\Gamma}_i$ appearing as a difference between the electron and ion fluxes.

4.1. Charged-particle fluxes

Figures 5 and 6 present, respectively, the direction and the magnitude of the charged-particle fluxes and also a quantitative comparison of the components—radial and axial—of the electron and ion fluxes. The main conclusion from figures 5(*a*) and (*b*) and figures 6(*a*)–(*c*) is that the electron and ion fluxes are different both in their direction and magnitude. Therefore, a flux

$$\mathbf{\Gamma} = \mathbf{\Gamma}_e - \mathbf{\Gamma}_i \tag{13}$$

appears which means that a net current exists in the discharge. As mentioned in section 2, this is permitted by the set of equations (2)–(4) and (9) provided

$$\mathrm{div}\mathbf{\Gamma} = 0. \tag{14}$$

A numerical check has confirmed that the obtained results for the fluxes in our case fulfil this requirement.

4.1.1. Qualitative description of the discharge formation. Ambipolar diffusion, i.e. equality of the electron and ion fluxes, is the expectation for the regime of the discharge maintenance in the pressure range considered here when the discharge vessel is with dielectric walls. Obviously, the metal walls of the discharge vessel, in combination with the different dimensions of the two chambers completing it, cause the appearance of a difference in the electron and ion fluxes, i.e. of the flux $\mathbf{\Gamma}$ and, respectively, of a dc current in the discharge.

The metal walls of the discharge vessel lead to the following qualitative picture of the discharge maintenance. At the discharge breakdown the electrons, due to their higher diffusibility, leave the discharge faster than the ions. As a result, the plasma charges positively and a dc potential builds up in the discharge. Because of the metal walls of the discharge vessel, the potential difference between the plasma and all the walls is the same. However, due to the different dimensions of the source in the radial and axial directions, the radial component of the electric field is higher than the axial one.

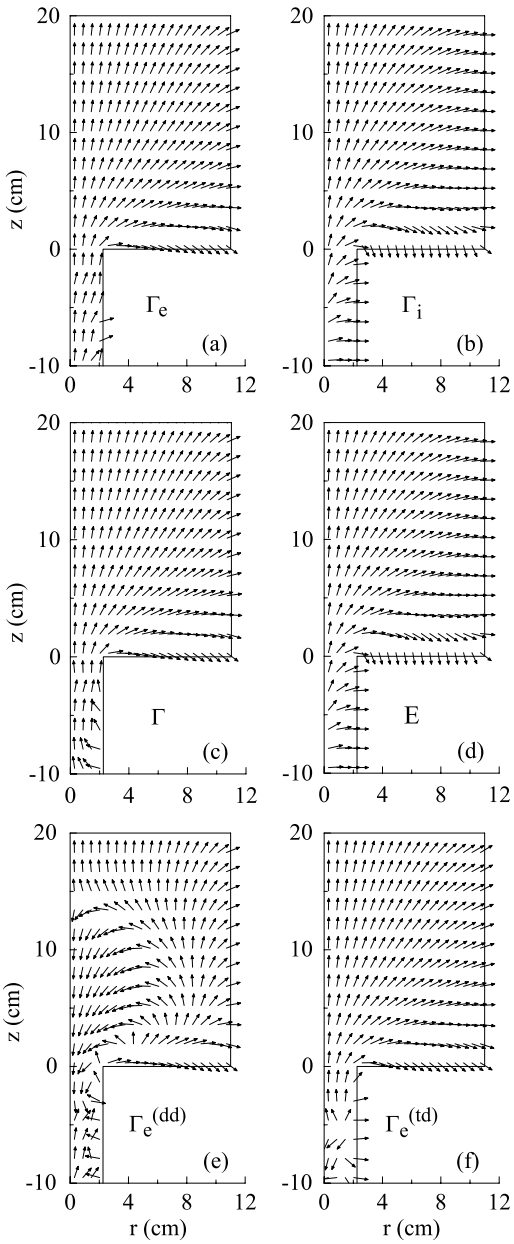

Figure 5. Arrow plot presentation of the direction of the fluxes of electrons ($\mathbf{\Gamma}_e$ in (*a*)) and ions ($\mathbf{\Gamma}_i$ in (*b*)), of the flux $\mathbf{\Gamma} = \mathbf{\Gamma}_e - \mathbf{\Gamma}_i$ (*c*) and of the electric field ($\boldsymbol{E}$ in (*d*)) as well as of the components of the electron flux: drift–diffusion flux ($\mathbf{\Gamma}_e^{(dd)}$ in (*e*)) and thermal diffusion flux ($\mathbf{\Gamma}_e^{(td)}$ in (*f*)), for gas pressure $p = 100$ mTorr. The plots cover the driver region starting from the position $z_0 = -10$ cm of the centre of the super-Gaussian profile of the input power and extend over the second chamber of expanding plasmas to almost half of its length.

The dc field is an accelerating field for the ions and a retarding field for the electrons. Its configuration in the driver favours a radial motion of the ions (figure 5(*b*)) towards the side walls and an axial motion of the electrons (figure 5(*a*)) towards the second chamber.

Thus, the different fluxes of electrons and ions to the walls of the discharge vessel (an electron flux through the second chamber and a radial ion flux in the driver) cause a current flowing from the second chamber to the driver which is short-circuited via the metal walls. Therefore, the different

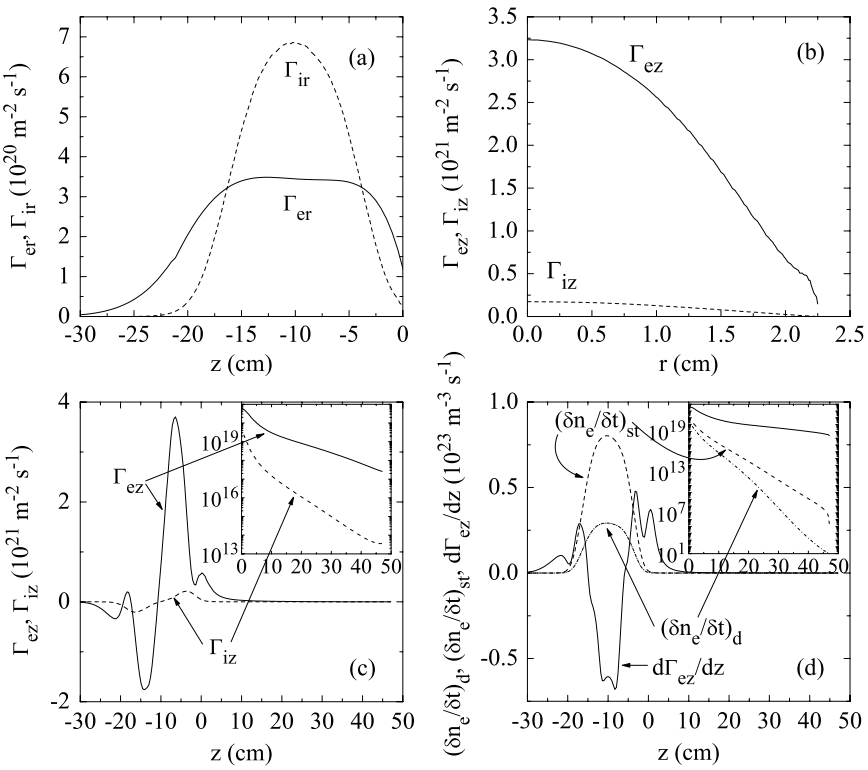

Figure 6. Axial variations of the radial components of the electron (Γ_{er}) and ion (Γ_{ir}) fluxes at the wall ($r \equiv R_1 = 2.25$ cm) of the first chamber in (*a*), radial variation (*b*) of the axial electron (Γ_{ez}) and ion (Γ_{iz}) fluxes at $z = -5$ cm and axial variation (*c*) of the same flux components at the discharge axis ($r = 0$). Axial variation at $r = 1$ cm of the contributors—step ionization $(\delta n_e/\delta t)_{st}$, direct ionization $(\delta n_e/\delta t)_d$ and $d\Gamma_{ez}/dz$—to the electron balance in (*d*); gas pressure $p = 100$ mTorr.

dimensions in the radial and axial directions of the discharge vessel and its metal walls lead to a net current in the plasma and, thus, to a diffusion regime of the discharge different from the regime of ambipolar diffusion and similar to Simon diffusion, well known [20] for discharges in metal vessels, but with an external magnetic field present.

The almost equal times of the electron flight $\tau_e = 3.6 \times 10^{-4}$ s at the axis of the discharge vessel and of the radial ion flight $\tau_i = 2.5 \times 10^{-4}$ s in the driver (at $z = -9$ cm) come as a confirmation of the above description of the discharge maintenance; $\tau_e = \int_{z_0}^{L_2} \frac{dz}{v_{ez}}$ and $\tau_i = \int_0^{R_1} \frac{dr}{v_{ir}}$ are calculated by using the numerical results obtained for the charged-particle velocities.

4.1.2. Presentation of the fluxes through the net flux $\mathbf{\Gamma}$ *in the discharge.* By presenting—via (13)—the electron flux $\mathbf{\Gamma}_e = \mathbf{\Gamma}_i + \mathbf{\Gamma}$ through the ion flux $\mathbf{\Gamma}_i$ and the flux $\mathbf{\Gamma}$ and after using expressions (5*a*) and (5*b*) for $\mathbf{\Gamma}_e$ and $\mathbf{\Gamma}_i$, the following form—useful for discussions on the numerical results—can be reached for the dc field and for the electron and ion fluxes in the discharge:

$$\boldsymbol{E} = \boldsymbol{E}_A + \frac{1}{b_e + b_i}\frac{\mathbf{\Gamma}_T}{n} - \frac{1}{b_e + b_i}\frac{\mathbf{\Gamma}}{n}, \tag{15a}$$

$$\mathbf{\Gamma}_e = \mathbf{\Gamma}_A + \frac{b_e}{b_e + b_i}\mathbf{\Gamma} + \frac{b_i}{b_e + b_i}\mathbf{\Gamma}_T, \tag{15b}$$

$$\mathbf{\Gamma}_i = \mathbf{\Gamma}_A + \frac{b_i}{b_e + b_i}(\mathbf{\Gamma}_T - \mathbf{\Gamma}). \tag{15c}$$

Here quasineutrality is assumed ($n_e = n_i = n$) and the ambipolar field and the ambipolar diffusion flux

$$\boldsymbol{E}_A = \frac{D_i - D_e}{b_i + b_e}\frac{\nabla n}{n}, \tag{16a}$$

$$\mathbf{\Gamma}_A = -\frac{b_i D_e + b_e D_i}{b_e + b_i}\nabla n, \tag{16b}$$

are introduced only as a notation;

$$\mathbf{\Gamma}_T = -D_e^T n_e \frac{\nabla T_e}{T_e} \tag{16c}$$

is the thermal diffusion flux. It is convenient to introduce $\mathbf{\Gamma}_A$, in order to have the same quantity ($\mathbf{\Gamma}_A$) staying in the expressions for the electron and ion fluxes.

4.1.3. DC electric field. The results obtained for the dc electric field in the discharge (figure 5(*d*)) confirm the qualitative description (section 4.1.1) of the discharge maintenance in the source. The radial dc electric field increases strongly, but smoothly, towards the walls ($r = R_1$ and $r = R_2$). The axial electric field is almost constant over the radius of the driver and it decreases towards the walls of the second chamber. Its maximum value, which is at the discharge axis, is orders of magnitude smaller than the radial field at the walls. Comparison with the $\boldsymbol{E}_A$ field (16*a*) shows that everywhere in the source the dc electric field formed in the discharge is close to $\boldsymbol{E}_A$ ($\boldsymbol{E} \simeq \boldsymbol{E}_A$). This concerns both its radial and

axial components. The contributions of the terms in (15*a*) related to $\mathbf{\Gamma}_T$ and $\mathbf{\Gamma}$ are quite smaller than $\boldsymbol{E}_A$. Thus, very small deviations of $\boldsymbol{E}$ from $\boldsymbol{E}_A$ lead to the difference $\mathbf{\Gamma}$ in the electron and ion fluxes and to the appearance of a net current in the discharge.

In fact, a retarding (for the electrons) field E_z smaller than the E_{Az} field, which is well pronounced in the driver, is the field forming the big axial flux of electrons towards the second chamber (figures 6(*b*) and (*c*)), which sustains the discharge there.

4.1.4. Electron and ion fluxes. Figure 5 where the directions of the fluxes (5*a*) and (5*b*) are given shows that the ion flux (figure 5(*b*)) follows the electric field (figure 5(*d*)) in the discharge. Besides the driver region, the electron flux (figure 5(*a*)) is in the direction of the flux $\mathbf{\Gamma}$ (figure 5(*c*)). In fact, the formation of the electron flux (5*b*) is complicated as it is shown by figures 5(*e*) and (*f*) where its components, i.e. the drift–diffusion flux of the electrons

$$\mathbf{\Gamma}_e^{(dd)} = -b_e n_e \boldsymbol{E} - D_e \nabla n_e \qquad (17a)$$

and their thermal diffusion flux

$$\mathbf{\Gamma}_e^{(td)} \equiv \mathbf{\Gamma}_T = -D_e^T n_e \frac{\nabla T_e}{T_e}, \qquad (17b)$$

are given separately. The complicated behaviour of the thermal diffusion flux (figure 5(*f*)) is in the driver where due to the maxima of T_e there, mentioned in section 3, a radial flux directed towards the axis and an axial flux directed towards the centre of the driver are formed. The two contributors to the electron drift–diffusion flux (17*a*), i.e. the drift flux $\mathbf{\Gamma}_e^{(d)} = -b_e n_e \boldsymbol{E}$ in the dc field and the diffusion flux $\mathbf{\Gamma}_e^{(dif)} = -D_e \nabla n_e$, being opposite in their directions are comparable in magnitude. This leads to different directions of the electron drift–diffusion flux (figure 5(*e*)) in the different regions of the discharge vessel. However, the thermal diffusion flux $\mathbf{\Gamma}_e^{(td)}$ (figure 5(*f*)), being quite smaller than both the diffusion and the drift fluxes, is large enough compared with their difference, especially in the transition region between the two chambers, where the electron temperature drops strongly (figure 3(*b*)). Having the same direction as that of the diffusion flux, the thermal diffusion flux takes care of removing the complications in the drift–diffusion flux (figure 5(*e*)) and finally ensuring a nice smooth behaviour of the total electron flux (figure 5(*a*)). Although playing an important role in the formation of the total electron flux, the thermal diffusion flux does not influence the discharge regime. Calculations carried out without accounting for the thermal diffusion flux show the same regime of discharge maintenance: a regime with a net dc current in the discharge. In this case the diffusion flux and the drift flux redistribute in a way that ensures almost the same total flux, both in its direction and magnitude as that given in figure 5(*a*), thus providing almost the same Γ flux (figure 5(*c*)). Expression (15*b*) also shows that the strong deviation of $\mathbf{\Gamma}_e$ from $\mathbf{\Gamma}_A$ is due to the flux $\mathbf{\Gamma}$, and not to the thermal diffusion flux $\mathbf{\Gamma}_T$ (due to the small (b_i/b_e) ratio in front of it).

In accordance with the qualitative description of the source operation in section 4.1.1, Γ_{ir} exceeds Γ_{er} in the driver (figure 6(*a*)). Also, in confirmation of this description Γ_{ez} in the driver (figures 6(*b*) and (*c*)) is quite larger than Γ_{iz}. In the second chamber, Γ_{ez} (figure 6(*c*)), as well as Γ_{er}, is larger than the corresponding components of the ion flux. This determines an electron flux both to the side wall ($r \equiv R_2 = 11$ cm) of the second chamber and to its back wall ($z = 47$ cm). In fact, the axial electron flux coming from the driver (figure 6(*b*)) is lost to the walls of the second chamber, sustaining the discharge there.

Everywhere in the two chambers of the source the ion flux $\mathbf{\Gamma}_i$ in both the radial and axial directions is approximately equal to the $\mathbf{\Gamma}_A$ flux (16*b*). The flux $\mathbf{\Gamma}$ and the thermal diffusion flux could not affect the total ion flux $\mathbf{\Gamma}_i$ because of the small value of the (b_i/b_e) ratio in the second term on the right-hand side of expression (15*c*). In fact, some influence of the thermal diffusion flux shows evidence in the regions of strong spatial variation of T_e. The flux $\mathbf{\Gamma}$ slightly influences the axial component of $\mathbf{\Gamma}_i$ in the driver.

All over the total source $\Gamma_{ez} \gg \Gamma_{iz} \simeq \Gamma_{Az}$ (figures 6(*b*) and (*c*)). The same also holds for the radial components of the fluxes in the second chamber ($\Gamma_{er} \gg \Gamma_{ir} \simeq \Gamma_{Ar}$). Keeping in mind that the ion flux $\mathbf{\Gamma}_i$ is approximately equal to $\mathbf{\Gamma}_A$, (15*b*) clearly shows that Γ_{ez} all over the source and Γ_{er} in the second chamber are determined by the corresponding components of the flux $\mathbf{\Gamma}$. The thermal diffusion flux $\mathbf{\Gamma}_T$ in (15*b*) could not influence $\mathbf{\Gamma}_e$ because of the small (b_i/b_e) ratio in front of $\mathbf{\Gamma}_T$ in (15*b*). The comparison of Γ_{ez} with Γ_{iz} (figures 6(*b*) and (*c*)) shows that the flux $\mathbf{\Gamma}$, having the same direction as $\mathbf{\Gamma}_A$, exceeds it with orders of magnitude. However, in the driver region $\Gamma_{er} < \Gamma_{ir} \simeq \Gamma_{Ar}$ (figure 6(*a*)). Analysis of the different contributors to Γ_{er} (15*b*) in the driver shows that the radial component of $\mathbf{\Gamma}$ is opposite in its direction to Γ_{Ar} and it is smaller in magnitude. Thus, the radial component of $\mathbf{\Gamma}_e$ in the driver is $\Gamma_{er} \simeq \Gamma_{Ar} - |\Gamma_r|$ and it is directed towards the walls.

4.1.5. Relation of the net flux $\mathbf{\Gamma}$ to the discharge parameters. Whereas $\mathbf{\Gamma}_A$ and $\mathbf{\Gamma}_T$ are expressed via (16*b*)–(16*c*) through the plasma parameters, the flux $\mathbf{\Gamma}$ stays in (15*a*)–(15*c*) as an external parameter. This raises the question as to which are the factors determining $\mathbf{\Gamma}$. Obviously, it should depend on the size and geometry of the discharge vessel. However, it is also obvious that an analytical expression for $\mathbf{\Gamma}$ could not be obtained when the geometry of the discharge vessel is as complicated as that of the source in figure 1. But estimations could be made considering only the driver region and replacing the exit to the second chamber by a metal wall. Equalizing the radial ion flux ($\Gamma_{ir} \simeq \Gamma_{Ar}$) to the side wall ($r \equiv R_1 = 2.25$ cm) and the total axial electron flux to the front ($z = 0$ cm) and back ($z = -30$ cm) walls of the first chamber results in the following expression:

$$\overline{\Gamma} = \mu J_1(\mu) \frac{L_1}{R_1^2} D_A \overline{n(z)}, \qquad (18)$$

for the axial flux $\overline{\Gamma}$ ($\overline{\Gamma} \simeq \overline{\Gamma_{ez}}$) averaged over the front and back walls. A Bessel type of a radial profile of the plasma density as shown to be valid (figure 4) is used. Expression (18) shows that the flux $\mathbf{\Gamma}$ depends on both the plasma parameters (D_A and n) and the dimensions—length and radius—of the discharge vessel.

4.1.6. Comparison of the contributors to the electron balance. Figure 6(*d*) shows the axial variation of the contributors—direct $(\delta n_e/\delta t)_d$ and step $(\delta n_e/\delta t)_{st}$ ionization and axial electron flux $d\Gamma_{ez}/dz$—to the electron balance (2). The contribution of the radial component of the electron flux is not shown because it appears always as electron losses at the walls. The obtained results show plasma production by step and direct ionization in the driver, i.e. in the region of the power input. The step ionization strongly exceeds the direct ionization as it is expected [28, 30, 31] for the gas pressure of 100 mTorr considered, when the electron density, respectively, the applied power, is high enough. The axial electron flux appears as electron losses in the driver region and a source of electrons in the expanding plasma region. Such a result is in accordance with the results for the directions and the magnitudes of the fluxes already discussed. The most important conclusion is that the influx of electrons in the second chamber from the first one strongly exceeds the charged particle production there via direct and step ionization.

The obtained results lead to the conclusion that the plasma existence in the expanding plasma region is due to charged-particle fluxes from the driver. There is a strong electron flux flowing over an ion background. Since the condition of quasineutrality is fulfilled, except for the wall sheath, as usual, different electron and ion fluxes mean quite different velocities of electrons and ions, as the results show. The latter is an indication of the importance of the dc field in the source. As the next subsection shows, the electron energy in the expanding plasma volume is lost for its maintenance.

4.2. Electron-energy flux

Figures 7 and 8 show the orientation, the magnitude and the spatial distribution of the electron-energy flux $\boldsymbol{J}$ and its constituents: the conductive flux $\boldsymbol{J}^{(\mathrm{cond})}$ and the convective flux $\boldsymbol{J}^{(\mathrm{conv})}$. The spatial variations of the different contributors to the electron-energy balance (3) are shown in figure 9.

4.2.1. General behaviour of the flux and its constituents. In general, the electron-energy flux (figure 7(*a*)), similarly to the electron flux, is a forward flux, directed from the driver towards the expanding plasma volume, with a strong orientation towards the walls, close to them.

The pattern of the conductive flux $\boldsymbol{J}^{(\mathrm{cond})}$ in the driver region is more complicated due to the appearance of the maxima of T_e, in both the radial (at $r_{max} = 1.35$ cm) and the axial (at $z_{max} = -7.5$ cm) directions, discussed in section 3. From the positions (r_{max} and z_{max}) of each maximum, conductive fluxes flow in both directions: radial fluxes both towards the walls and towards the axis as well as both forward and backward axial fluxes. This means changing the signs of both the radial and axial components of $\boldsymbol{J}^{(\mathrm{cond})}$. For $J_z^{(\mathrm{cond})}$, this is shown in figure 8 by the three zero points of this flux at the centre z_0 of the power input and at both sides of the centre, close to the edges of the region of the power deposition.

However, since the convective flux is a forward flux (figures 7(*c*) and 8), i.e. always—over the total length of the source—directed from the power input region towards the

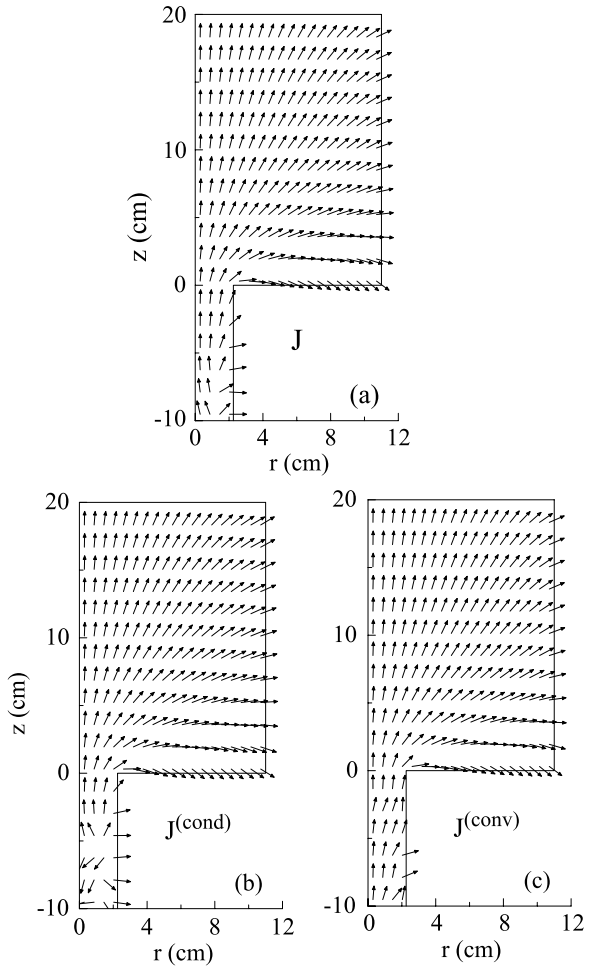

Figure 7. Arrow plot presentation of the direction of the electron-energy flux (*a*) and its constituents: the conductive (*b*) and convective (*c*) fluxes. The plots cover the driver region starting from the position $z_0 = -10$ cm of the centre of the super-Gaussian profile of the power input and extend over the second chamber of expanding plasmas to almost half of its length; gas pressure $p = 100$ mTorr.

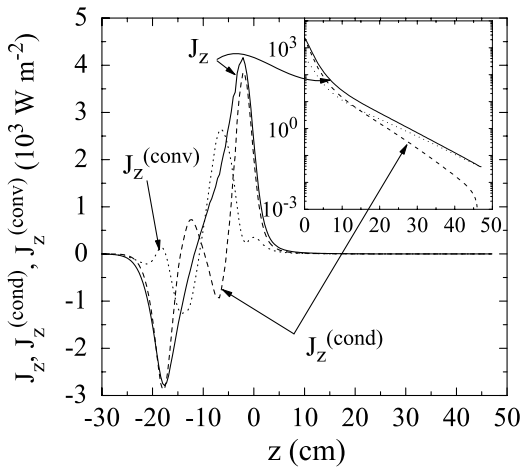

Figure 8. Axial variation at the discharge axis of the axial component of the electron-energy flux $\boldsymbol{J}$ and its constituents: the conductive $\boldsymbol{J}^{(\mathrm{cond})}$ and convective $\boldsymbol{J}^{(\mathrm{conv})}$ fluxes; gas pressure $p = 100$ mTorr.

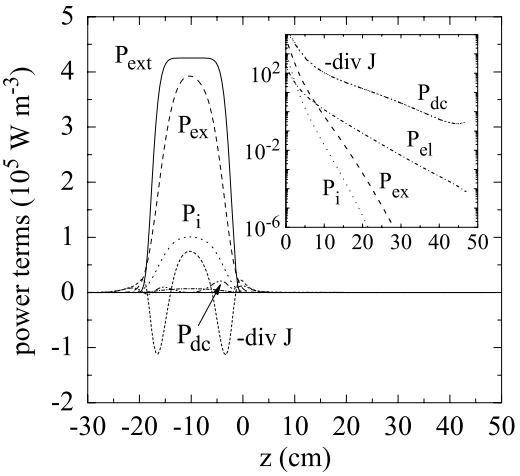

Figure 9. Axial variations of the contributors along the discharge axis ($r = 0$) to the electron-energy balance (3). The notation used are externally applied power P_{ext}, electron energy losses in collisions for atom excitation P_{exc} and ionization P_i and in elastic electron–neutral collisions P_{el} as well as electron energy losses P_{dc} for maintenance of the dc field in the discharge; gas pressure $p = 100$ mTorr.

expanding plasma region and its axial component $J_z^{(conv)}$ in the driver is larger than $J_z^{(cond)}$, the total flux J_z (figure 7(*a*)) in the driver follows the convective flux, i.e. it is a forward flux. At the edge of the driver towards the transition to the second chamber of the source the axial component $J_z^{(cond)}$ of the conductive flux strongly increases (figure 8), due to the strong drop in T_e there (figure 3(*b*)). In this region $J_z^{(cond)}$ constitutes almost completely the total energy flux $\boldsymbol{J}$ (figure 8). However, in this region $J_z^{(cond)}$ is a forward flux ensuring electron-energy input to the expanding plasma volume. Deep in the expanding plasma region the total energy flux $\boldsymbol{J}$ (figure 8) decreases with increasing distance from the driver.

4.2.2. Analysis of the contributors to the electron-energy balance. The role of the three terms on the right-hand side of the electron-energy balance (3) is completely clear: P_{ext} is the external power input localized in the driver and P_{coll} and $P_{dc} = -e\boldsymbol{\Gamma}_e \cdot \boldsymbol{E}$ are electron-energy losses everywhere in the plasma source, respectively, in collisions and for the maintenance of the dc electric field in the discharge. The role of the (div$\boldsymbol{J}$) term on the left-hand side of (3) is more complicated because it plays a different role in the different regions of the source. Moreover, the two constituents of the electron-energy flux—$\boldsymbol{J}^{(cond)}$ and $\boldsymbol{J}^{(conv)}$—play a different role even in one and the same region of the source.

In the driver region $\boldsymbol{J}^{(conv)}$ directs electron energy away from the driver towards the second chamber in the axial direction and towards the walls, in the radial direction (figure 7(*c*)). The result is that the (div$\boldsymbol{J}^{(conv)}$) part of the (div$\boldsymbol{J}$) term as a whole (through both $J_r^{(conv)}$ and $J_z^{(conv)}$) appears as electron-energy losses in the driver. Due to the complicated behaviour of $\boldsymbol{J}^{(cond)}$ in the driver, already discussed, the (div$\boldsymbol{J}^{(cond)}$) part of the (div$\boldsymbol{J}$) term in the region $z \lesssim -7.5$ cm of the driver appears as a power input in the vicinity of the discharge axis and as power losses close to the walls. Thus, in the central part of the driver in the region around the discharge axis power deposition ensured externally and through the conductive flux compensates electron-energy losses through collisions (figure 9). Among the losses through collisions, the losses for atom excitation strongly exceed the losses for ionization as it is expected in active parts of discharges, for the gas pressure considered [28, 30, 31]. Due to the comparatively low gas pressure [28], the losses in elastic collisions are negligible.

The axial electron-energy flux $\boldsymbol{J}$ from the driver, with its two constituents (axial conductive and convective fluxes), is the power input to the expanding plasma volume (figure 9). In accordance with figure 6(*d*), the power losses for ionization are negligible. The power losses in elastic and inelastic collisions for excitation are also negligible. In fact, the main and the most important losses are those for maintenance of the dc field in the expanding plasma region.

This leads to the basic conclusion that the particle fluxes from the driver ensure the plasma existence in the expanding plasma volume. The electron-energy input carried by the electron flux goes for compensating the losses for maintenance of the dc field in the discharge. On the other hand, this field controls the electron flux.

Calculations of the electron-energy losses in the source show that 96% of the input power (100 W) is lost in the driver. The losses through collisions in the plasma volume and for maintenance of the dc field take 86% of the input power. The rest is taken by the convective flux at the walls. The main contributors to the losses in the plasma volume are the losses for atom excitation (37%) and the losses for maintenance of the dc field there (35%). Only 4% of the input power goes—through the electron-energy flux from the driver—towards sustaining the plasma in the expansion plasma volume. The maintenance of the dc field there takes 2.8% of the input power and 1% is the power lost through the convective flux to the walls.

5. What would happen if an ambipolar-diffusion regime were assumed?

The results discussed in the previous sections show that the metal walls of the discharge chamber, in combination with the discharge geometry, determine a discharge regime different from the ambipolar-diffusion regime. The ion flux is almost equal to the ambipolar-diffusion flux. However, the electron flux strongly exceeds it all over the source except for the radial electron flux in the driver which is below the ambipolar flux. Thus, there is a strong electron flux which sustains the expanding plasma of the discharge and a net dc current flowing through the discharge. Moreover, an electric field slightly deviating from the ambipolar field determines this flux. There is almost no charged-particle production in the expanding plasma volume. The electron-energy flux in this region compensates the losses for maintenance of the dc field there which, from the other side, ensures the charged-particle fluxes that provide the plasma existence there.

With the results briefly discussed here we would like to show what would be the predictions for the discharge behaviour if an ambipolar-diffusion regime were initially assumed.

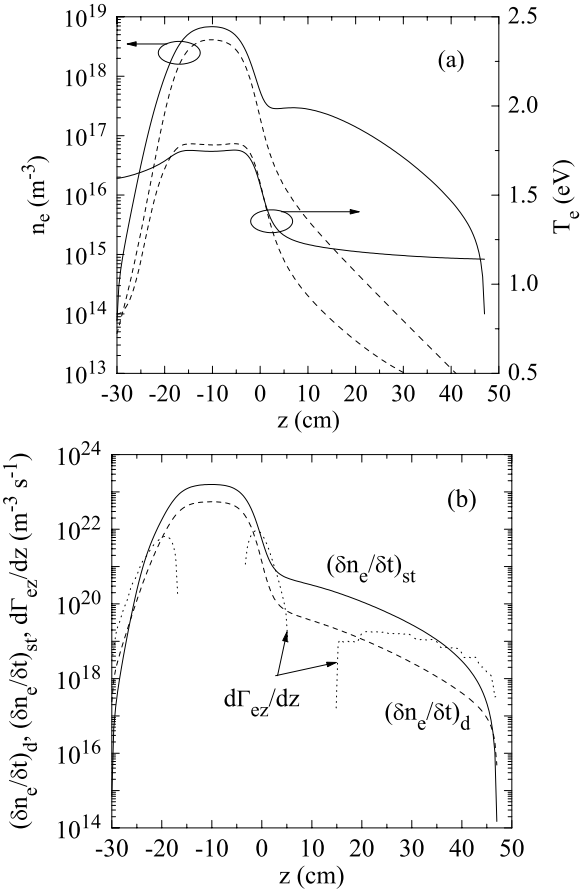

Figure 10. Axial variation at the discharge axis ($r = 0$) of the plasma density and electron temperature ((*a*) in solid curves) and of the contributors—step ionization $(\delta n_e/\delta t)_{st}$ and direct ionization $(\delta n_e/\delta t)_d$ and $d\Gamma_{ez}/dz$—to the electron balance (*b*) obtained within the assumption for an ambipolar-diffusion regime; gas pressure $p = 100$ mTorr. By dashed curves in (*a*) the results shown in figures 3(*a*) and (*b*) obtained in the regime of a net current in the discharge are given for comparison.

Now the set of equations numerically solved includes (i) the continuity equations (2) for electrons and ions reduced—through an assumption for equality of the ion and electron flux—to an electron balance equation with an electron flux including both diffusion and thermal diffusion fluxes, (ii) the electron-energy balance equation (3) and (iii) the balance equation of the excited atoms (9). The condition for quasineutrality replaces the Poisson equation. The Bohm criterion is the boundary condition for the ions at the walls ($v_i^{(wall)} = v_s$ where v_s is the ion acoustic velocity).

Figure 10 shows the results obtained for the axial variation at the discharge axis ($r = 0$) of the plasma density, the electron temperature and of the contributors to the electron balance.

The comparison (figure 10(*a*)) of the axial variation of T_e with the corresponding result in figure 3(*b*) shows that both in trends of variation and values, the behaviour of the electron temperature in the driver is almost the same both in the ambipolar-diffusion regime and in the regime with a net current in the source. The transition region which covers the edge of the power input region and the beginning of the expanding plasma region also shows similar behaviour in the two regimes. However, the $T_e(z)$ variations in the expanding plasma regions are completely different. The ambipolar-diffusion-regime sustained plasmas have a quite higher temperature which is almost constant in the z-direction. The temperature drop in the regime with a net current in the plasma is extended over the total length of the expanding plasma volume.

The comparison (figure 10(*a*)) of the axial profiles of the plasma density obtained within the two regimes—the ambipolar-diffusion regime and the regime with a net dc current in the discharge—also shows essential differences, again in the expanding plasma volume. Instead of the almost exponential drop in the plasma density in the regime with a net current in the plasma, the ambipolar-diffusion regime shows up with the formation of a plateau in the $n_e(z)$ profile at the beginning of the expanding plasma volume followed by a comparatively fast decrease in $n_e(z)$ which ends with a very fast drop in the density at the back wall ($z = 47$ cm) of the second chamber. The ambipolar-diffusion regime predicts about two orders of magnitude higher plasma density in the expanding plasma region (the second chamber of the discharge vessel) than the regime with a net current in the source. In general, figure 10(*a*) shows that both T_e and n_e in the driver (where the external power is applied) are the same in the two regimes. The differences are in the expanding plasma region where the discharge maintenance is controlled by the fluxes and it is the fluxes that appear to be quite different in the two regimes.

Whereas the charged-particle production in the expanding plasma volume of the regime with a net current in the source is negligible (more than 5 orders of magnitude lower for $z > 10$ cm) compared with the contribution of the ($\mathrm{div}\boldsymbol{\Gamma}_e$) term in the electron balance (figure 6(*d*)), in the ambipolar-diffusion regime they are comparable (figure 10(*b*)). Thus, the ambipolar-diffusion regime predicts plasma maintenance in the expanding plasma volume by charged-particle production there, not only by the electron flux from the driver as it is in the regime with a net current in the source. The ambipolar flux from the driver is quite lower than the electron flux in the regime with a net current in the source (where $\Gamma_e \simeq \Gamma \gg \Gamma_A$) and it could not ensure the plasma existence in the expanding plasma volume. Therefore, it is necessary to have an ionization there. This requires a higher electron temperature as appears in figure 10(*a*).

With the low electron flux in the ambipolar-diffusion regime, the convective flux is low and the electron-energy flux is a conductive flux. The thermal conductivity does not permit temperature changes and the electron temperature stays almost constant (figure 10(*a*)). Moreover, the high thermal conductivity does not permit a strong difference in the electron temperature in the driver and in the expanding plasma volume. This leads to the higher electron temperature in the ambipolar-diffusion regime. The latter supports ionization in the expanding plasma volume. This leads to a higher plasma density (figure 10(*a*)), which ensures a higher thermal conductivity coefficient and, respectively, a higher thermal flux.

Therefore, high electron flux and, respectively, importance of the convective flux mark the regime with a net current in the plasma whereas low ambipolar flux appearing in a combination with importance of the conductive flux characterizes the ambipolar-diffusion regime.

6. Conclusions

Through the model for the operation of tandem plasma sources with metal walls and different sizes of the two chambers of their vessel, presented here, a regime of discharge maintenance different from the ambipolar-diffusion regime is found. The metal walls keeping the same dc potential and different dimensions in the transverse and longitudinal directions of the discharge vessel lead to the establishment of a dc electric field in the discharge which, although only slightly deviating from the ambipolar field, has a strong impact on the discharge behaviour, through the charged-particle fluxes. Ions and electrons flow in different directions which results in a net dc current in the discharge (a high-frequency discharge), short-circuited through the metal walls of the vessel. In fact, a retarding longitudinal electric field smaller than the corresponding ambipolar field forms a strong axial flux of electrons from the driver towards the expanding plasma volume of the source and ensures the plasma maintenance there. The energy flux carried by the electron flux—a convective flux—serves to sustain the dc field in the expanding plasma volume, needed for the maintenance of the net current in the discharge.

A further extension of the work will be towards modelling the source operation in hydrogen gas with regard to the use of the inductively driven tandem-type of discharges as sources of negative ion beams for additional heating in fusion.

Acknowledgments

The work is within the programme of the Bulgarian Association EURATOM/INRNE (task P2) and the Project 3.4-Fokoop-BUL/10 26 323 supported by the Alexander-von-Humboldt Foundation.

References

[1] Holmes A J T 1992 *Plasma Phys. Control. Fusion* **34** 653
[2] Kushner M J 1993 *J. Appl. Phys.* **73** 4098
[3] Boeuf J P and Pitchford L C 1995 *Phys. Rev.* E **51** 1376
[4] Lymberopoulos D P and Economou D J 1995 *J. Res. Natl Stand. Technol.* **100** 473
[5] Pérès I and Kushner M J 1996 *Plasma Sources Sci. Technol.* **5** 499
[6] Ramamurthi B and Economou D J 2002 *Plasma Sources Sci. Technol.* **11** 324
[7] Hagelaar G L M, Bareilles J, Garrigues L and Boeuf J-P 2002 *J. Appl. Phys.* **91** 5592
[8] Subramonium P and Kushner M J 2002 *J. Vac. Sci. Technol.* A **20** 313
[9] Kushner M J 2003 *J. Appl. Phys.* **94** 1436
[10] Hagelaar G L M 2007 *Plasma Sources Sci. Technol.* **16** S57
[11] Bacal M 1989 *Nucl. Instrum. Methods Phys. Res.* B **37–38** 28
[12] Lymberopoulos D P and Economou D J 1993 *Appl. Phys. Lett.* **63** 2478
[13] Lymberopoulos D P and Economou D J 1994 *J. Vac. Sci. Technol.* A **12** 1229
[14] Salabas A, Gousset G and Alves L L 2002 *Plasma Sources Sci. Technol.* **11** 448
[15] Kinder R L and Kushner M J 2001 *J. Appl. Phys.* **90** 3699
[16] Kinder R L, Ellingboe A R and Kushner M J 2003 *Plasma Sources Sci. Technol.* **12** 561
[17] Ventzek P L G, Grapperhaus M and Kushner M J 1994 *J. Vac. Sci. Technol.* B **12** 3118
[18] Ventzek P L G, Hoekstra R J and Kushner M J 1994 *J. Vac. Sci. Technol.* B **12** 461
[19] Shahid R and Kushner M J 1997 *J. Appl. Phys.* **82** 2805
[20] Golant V E, Zhilinskiy A P and Sakharov A J 1997 *Fundamentals of Plasma Physics* (Moscow: Atomizdat) (in Russian)
[21] Speth E *et al* 2006 *Nucl. Fusion* **46** S220
[22] Kiss'ovski Zh, Kolev St, Shivarova A and Tsankov Ts 2007 *IEEE Trans. Plasma Sci.* **35** 1149
[23] Hagelaar G I M, de Hoog F J and Kroesen G M W 2000 *Phys. Rev.* E **62** 1452
[24] Dimitrova M, Djermanova N, Kiss'ovski Zh, Kolev St, Shivarova A and Tsankov Ts 2006 *Plasma Process. Polym.* **3** 156
[25] Tsankov Ts, Kiss'ovski Zh, Djermanova N and Kolev St 2006 *Plasma Process. Polym.* **3** 151
[26] Djermanova N, Kiss'ovski Zh, Lishev St and Tsankov Ts 2007 *J. Phys: Conf. Ser.* **63** 012013
[27] Iordanova S and Koleva I 2007 *Spectrochim. Acta* B **62** 344
[28] Kolev St, Schlüter H, Shivarova A and Tarnev Kh 2006 *Plasma Sources Sci. Technol.* **15** 744
[29] Kolev St, Lishev St, Shivarova A, Tarnev Kh and Wilhelm R 2007 *Plasma Phys. Control. Fusion* **49** 1349
[30] Aliev Yu A, Schlüter H and Shivarova A 2000 *Guided-Wave Produced Plasmas* (Berlin: Springer)
[31] Schlüter H and Shivarova A 2007 *Phys. Rep.* **443** 121